Asian Journal of Chemistry; Vol. 36, No. 8 (2024), 1821-1828

ASIAN JOURNAL OF CHEMISTRY

https://doi.org/10.14233/ajchem.2024.31767

Nanogold Supported Titania Loaded SBA-15: An Efficient Catalyst for Reduction of 4-Nitrophenol

SOUMINI CHANDRALAYAM[1,*] and SUGUNAN SANKARAN[2]

[1]Department of Chemistry, M.E.S. Keveeyam College, Valanchery, Malappuram-676552, India
[2]Department of Applied Chemistry, Cochin University of Science and Technology, Cochin-682022, India

*Corresponding author: E-mail: souminic@meskeveeyamcollege.ac.in

Received: 21 April 2024; *Accepted*: 4 June 2024; *Published online*: 25 July 2024; AJC-21703

Gold nanoparticles with an average particle size below 5 nm were effectively dispersed over titania loaded SBA-15. The nanogold supported systems were found to be highly effective in the liquid phase reduction of 4-nitrophenol to 4-aminophenol at room temperature (304 K) obeying pseudo-first-order kinetics. The highly effective catalyst with 3 wt.% Au incorporation to 20 wt.% Ti loaded SBA-15 (3Au/20Ti/SBA) showed a TON of 5.8×10^{21} molecules/g and a TOF of 6.5×10^{18} molecules/g/s in the reaction.

Keywords: SBA-15, Gold nanoparticles, Reduction of 4-nitrophenol.

INTRODUCTION

Synthesis of 4-aminophenol (4-AP) is of much interested area as it is an important intermediate for the manufacture of antipyretic drugs, analgesics, dyestuffs, corrosion inhibitor, photographic developer, *etc*. [1]. Several reports are available on the catalytic reduction of 4-nitrophenol (4-NP) using nanoparticles of noble metals at room temperature and atmospheric pressure in water medium using sodium borohydride as reductant [2-6]. Supported gold nanoparticles are of great importance in this regard because of its stability, size related properties, *etc*.

Mesoporous silica is an attractive catalyst support due to its large surface area, high thermal stability, tunable pore size, diverse morphologies, *etc*. [7,8]. It is acidic in nature with low isoelectric point (~2) which hardly allows the adsorption of $[Au(OH)_xCl_{4-x}]^-$ anions [9,10]. In order to modify the surface properties of mesoporous silica, some functional groups have to be introduced onto the channel walls. Usually, organic functional moieties containing polar head groups like –SH, $–NH_2$, *etc*. are incorporated into it to stabilize gold nanoparticles and to prevent particle agglomeration [11,12]. Another method is to introduce metal oxides with high isoelectric point like titania, ceria, *etc*. either by wet impregnation or by co-synthesis method [7,13].

In present study, we have modified the surface of mesoporous SBA-15 with titania *via* simple wet impregnation method and then gold nanoparticles were effectively dispersed onto the developed material *via* deposition precipitation method. The catalysts were characterized using various physico-chemical techniques to identify the active phase accountable for catalysis. In comparison with earlier reports, the system with 3 wt.% Au incorporated on 20 % Ti loaded SBA-15 exhibited higher activity with a lower gold to 4-nitrophenol (4-NP) ratio (1/66) and also with a lower 4-NP to $NaBH_4$ ratio (1/53).

EXPERIMENTAL

Preparation of SBA-15: SBA-15 was prepared according to a reported procedure [14]. Typically 4.4 g of triblock copolymer P123 (Sigma-Aldrich, USA) was dispersed in 30 mL distilled water and stirred for 1.5 h. To the resultant solution, 120 g of 2 M HCl (Nice Chemicals, India) was added under stirring which was continued for 2 h. Finally, 9 g of tetraethyl orthosilicate (TEOS, Sigma-Aldrich) was added dropwise and the mixture was kept for aging at room temperature for 24 h. The resultant mixture was submitted to hydrothermal treatment at 100 ºC for 48 h. The product obtained was filtered, washed with distilled water and dried in air for 24 h followed by drying at 70 ºC in an air oven for 12 h. It was then calcined at 450 ºC for 8 h.

Preparation of titania loaded SBA: Titania loading was done by simple impregnation method in which titanium isopro-

poxide in isopropanol (0.1 M) was selected as the precursor material. The precursor solution was taken in such a way to get 20 wt.% of Ti on SBA-15. 10 g SBA-15 was added to this solution, followed by heating at 80 ºC for removal of the solvent. The concentrated sample was then dried in an oven at 85 ºC for overnight followed by calcination at 450 ºC for 3 h. The sample was denoted as 20Ti/SBA.

Gold loading: Chloroauric acid ($HAuCl_4 \cdot 3H_2O$, Sigma Aldrich) solution (3×10^{-3} M) was taken as precursor for the incorporation of gold on 20Ti/SBA and the percentage loading was varied from 1 to 4 weight % of Au over the support. Here, 20Ti/SBA was added to the chloroauric acid solution and pH of the solution was adjusted to nearly 8 by dropwise addition of 0.1 M NaOH (Merck) solution. It was stirred at 80 ºC for 1 h and then cooled to room temperature. The contents were filtered and washed with distilled water till the filtrate was free from chloride ions. The product was dried at 110 ºC for 18 h and calcined at 200 ºC for 2 h. Gold supported 20Ti/SBA was denoted as XAu/20Ti/SBA, where X denotes the percentage weight of Au incorporated to 20Ti/SBA. Au doped TiO_2 system ($3Au/TiO_2$) was also prepared for comparison.

Preparation of nanogold supported titania system ($3Au/TiO_2$): Titanium isopropoxide (3.8 mL) was added dropwise to 100 mL of isopropanol under sonication and the sonication was continued for 20 min. Approximately 10 mL of water was added dropwise to the above solution. It was stirred for 24 h, transferred to an autoclave and treated at 180 ºC for 1 day. The product was washed with water and dried at 100 ºC for 12 h. The system was represented as TiO_2. Then 3 wt.% of gold was supported on the TiO_2 system by the same procedure and the prepared system is represented as $3Au/TiO_2$.

Catalyst characterization: The prepared catalysts were characterized by ICP-AES, XRD, TEM, UV-vis DRS, BET surface area-pore volume measurements and XPS analyses. The ICP-AES measurements was conducted using simultaneous ICP wpectrometer (SPECTRO Analytical Instruments GmbH, Germany) with CCD detector. The wide angle XRD was recorded using Bruker AXS D8 Advance diffractometer employing a scan rate of 0.02º/s with Ni filtered Cu$K\alpha$ radiation source (λ = 1.54 Å). Low angle XRD of SBA 15 was recorded for 2θ between 0.5º and 3º on a Rigaku MiniFlex 600 Benchtop X-ray diffractometer with Cu$K\alpha$ radiation (λ = 1.54 Å). TEM analysis was performed using an ultra-high resolution analytical electron microscope JEOL 3010. The UV-vis DRS of the prepared samples were taken on Spectro UV-vis Double beam UVD-500 spectrophotometer equipped with an integrating sphere assembly with a charge coupled device detector. The scan range was 200-800 nm using $BaSO_4$ as internal standard. The surface area, pore volume and pore size distribution of the samples were carried out in a Micromeritics Tristar 3000 surface area and porosity analyser. XPS analysis was performed using AXIS ULTRA X-ray Photoelectron Spectrometer (KRATOS ANALYTICAL) with C1s at 284.6 eV as an internal standard.

Catalytic activity studies: The reduction of 4-nitrophenol (4-NP) was carried out at the room temperature. In a typical procedure, 0.002 g of nanogold supported catalyst was taken in a 100 mL beaker and 8 mL distilled water was added. It was stirred for 3 min using a magnetic stirrer at a stirring rate of 300 rpm. Aqueous solution of 20 mL of 4-NP (1 mmol) was added to the above mixture and stirred for another 2 min. Freshly prepared aqueous solution of $NaBH_4$ (0.04 g in 3.3 mL distilled water) was added to the above mixture. After adding $NaBH_4$ solution, the colour of mixture turned dark yellow due to the formation of *p*-nitrophenolate ion. The characteristic peak of *p*-nitrophenolate ion at 400 nm decreased with the reaction time and a new peak at 290 nm appeared, which was assigned to 4-AP. The progress of the reaction as a function of time was monitored using a UV-vis spectrophotometer.

RESULTS AND DISCUSSION

The composition of the catalyst systems were calculated by ICP-AES analysis (Table-1). The results indicated the successful incorporation of both Au and Ti on the parent SBA system. The TEM images of pure SBA-15 showed (Fig. 1) well-ordered hexagonal arrays of mesochannels with homogeneous ordering. The existence of hexagonally ordered mesochannels in the modified systems indicated the retention of the structure of SBA-15 even after modification.

TABLE-1
ICP AES ANALYSIS DATA OF THE PREPARED CATALYSTS

Catalysts	Composition (weight %)			
	Theoretical		Experimental	
	Ti	Au	Ti	Au
20Ti/SBA	20	–	15.63	–
1Au/20Ti/SBA	20	1	15.45	0.69
2Au/20Ti/SBA	20	2	14.35	1.33
3Au/20Ti/SBA	20	3	14.37	1.96
4Au/20Ti/SBA	20	4	15.05	1.58

From the histograms, the average size of gold nanoparticles in XAu/20Ti/SBA systems was observed below 5 nm (Fig. 2), whereas the pore size of mesochannels of the prepared catalysts was found to be around 5.0 nm as obtained using BET surface area analysis method (Table-2). It proved the effective dispersion of gold nanoparticles over the support [7,12]. In case of $3Au/TiO_2$ system, the average gold particle size was found to be higher than 6 nm (Fig. 2). It could be attributed to the low surface area of the titania support.

TABLE-2
TEXTURAL PROPERTIES OF THE PREPARED CATALYSTS

Catalytic system	BET surface area (m^2/g)	Pore volume (cm^3/g)	Pore diameter (nm)
Pure SBA-15	872.9	1.26	5.78
20Ti/SBA	593.8	0.72	4.86
1Au/20Ti/SBA	506.9	0.71	5.64
2Au/20Ti/SBA	535.9	0.67	4.99
3Au/20Ti/SBA	483.4	0.63	5.24
4Au/20Ti/SBA	497.6	0.64	5.17
TiO_2	160.3	0.52	5.64
$3Au/TiO_2$	139.6	0.47	5.94

XRD studies: The hexagonal arrangement of SBA-15 catalyst was confirmed by the low-angle XRD patterns (Fig. 3a). Three peaks at 1.08º, 1.65º, 1.91º for pure SBA-15 corres-

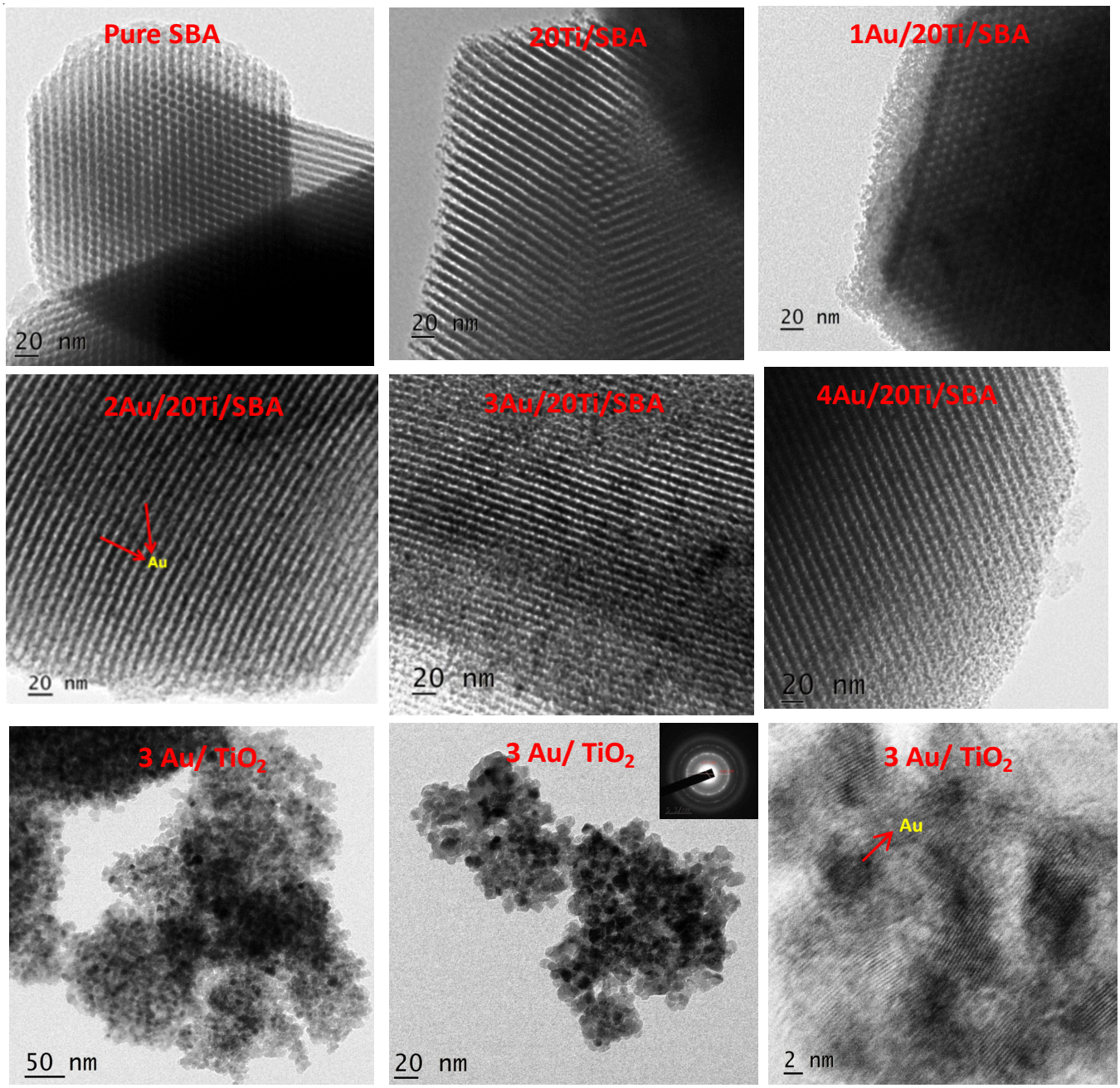

Fig. 1. TEM images of nanogold supported systems

ponded to the reflections from (100), (110) and (200) planes, respectively. These peaks were attributed to the hexagonal space group (*P6mm*) of mesoporous SBA-15 which indicated well-ordered packed channels of the sample [15,16]. The retention of these three peaks for XAu/20Ti/SBA systems indicated the retention of the hexagonal mesostructure of SBA-15 even after modification.

Presence of amorphous silica was evidenced from the wide angle XRD analysis (Fig. 3b). An intense broad peak around 2θ value of 25º corresponded to anatase titania. It was broadened due to merging with the peak of amorphous silica at 2θ value of around 22.5º. The peak at 2θ = 38º for XAu/20Ti/SBA corresponded to the (111) planes of FCC crystallized gold. The peaks at 2θ values 44.3º, 64.7º and 77.6º corresponding to the (200), (220) and (311) planes of FCC crystallized gold were very weak or absent. These weak diffraction lines for gold supported catalyst were attributed to the very low concentration or efficient dispersion and/or small particle size of nanogold in mesoporous silica [7]. The existence of anatase phase of titania in TiO_2 and $3Au/TiO_2$ systems was evidenced from the wide angle XRD patterns (Fig. 3c). The most intense peak of FCC crystallized gold at 2θ value of 38.4º was found to get merged with the anatase peak (at 38.1º) of titania. The weak intense peak at 2θ value of 44.3º for $3Au/TiO_2$ represented the presence of (200) planes of FCC crystallized gold.

Diffuse reflectance UV-vis studies: In the UV-vis diffuse reflectance spectra of modified SBA-15, the two bands nearly in the range of 215 nm and 275 nm corresponded to the charge

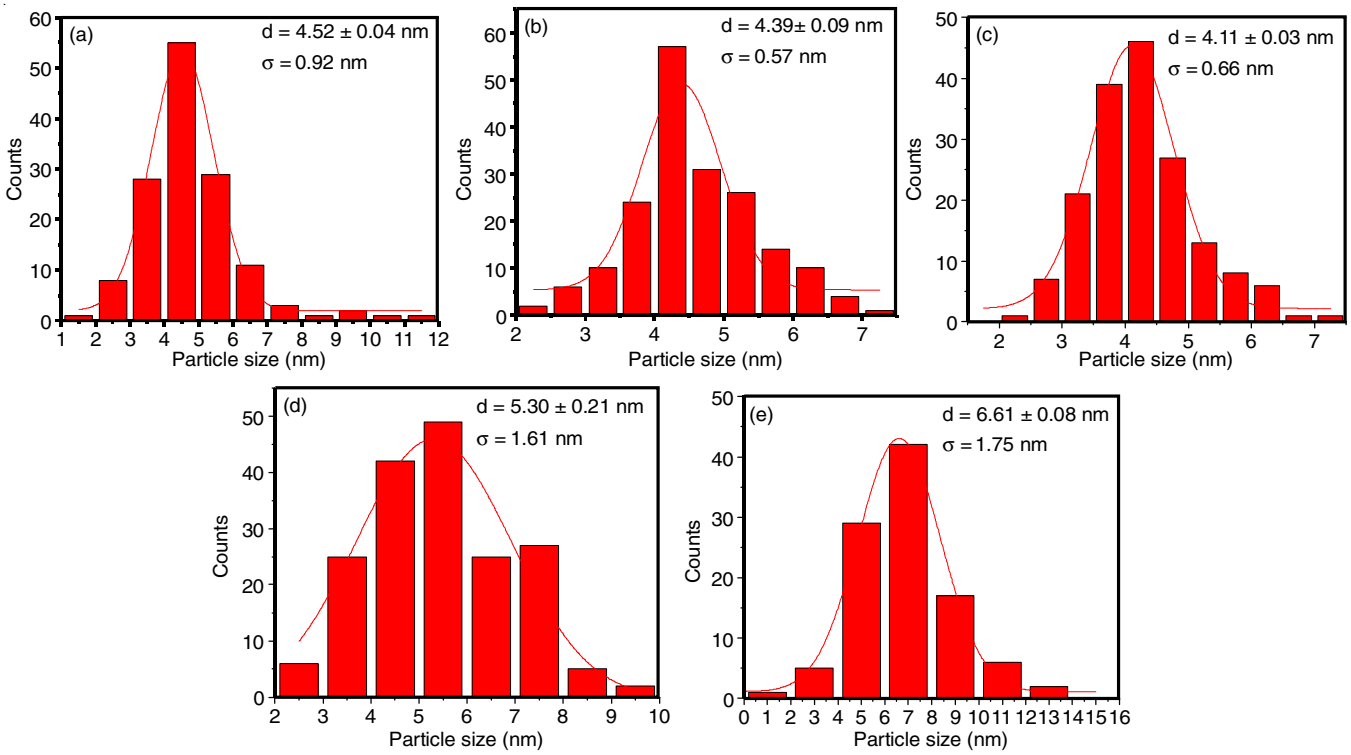

Fig. 2. Particle size distribution curves of (a) 1Au/20Ti/SBA, (b) 2Au/20Ti/SBA, (c) 3Au/20Ti/SBA, (d) 4Au/20Ti/SBA and (e) 3Au/TiO_2

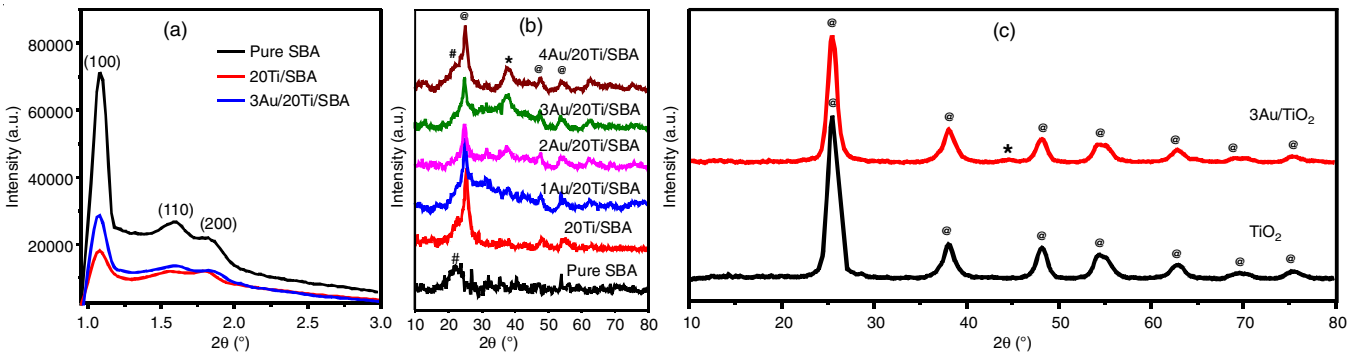

Fig. 3. (a) Small angle XRD of pure SBA-15, 20Ti/SBA and 3Au/20Ti/SBA, (b) wide angle XRD of SBA, 20Ti/SBA and XAu/20Ti/SBA samples (# SBA, @ TiO_2, * Au) and (c) wide angle XRD of TiO_2 and 3Au/TiO_2 (@ TiO_2, * Au)

transfer transitions between Ti^{4+} tetrahedral site and oxygen and the presence of partially polymerized Ti species, respectively (Fig. 4). In case of TiO_2 and 3Au/TiO_2 systems, the band at around 310 nm corresponded to the presence of free anatase titania [7]. The gold supported samples were characterized by a new broad peak around 513 nm, which indicated the surface plasmon excitations of ultra structures of gold nanoparticles [17].

Textural properties: The pure SBA-15 and modified systems exhibited type IV adsorption isotherms with H1 adsorption hysteresis loop indicating the capillary condensation of nitrogen in the mesopores (Fig. 5). The same shape of isotherm observed for both parent and modified samples implied that the mesostructure was retained even after modification. The shift of capillary condensation and adsorption desorption isotherm for modified samples to lower pressures could be ascribed to the mesochannel shrinkage after modification [18]. The surface

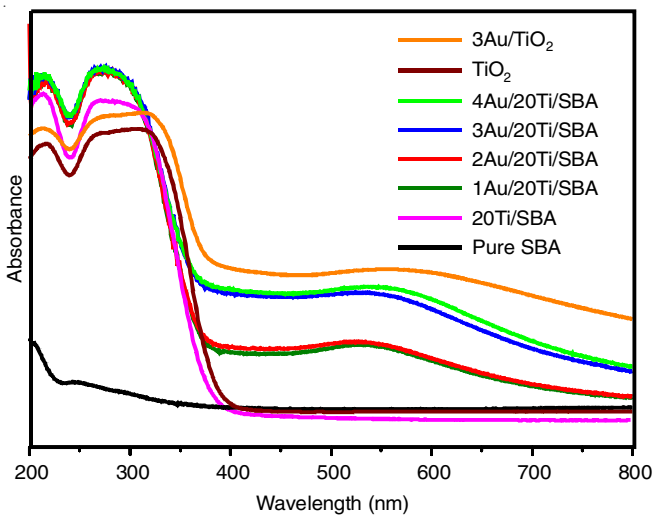

Fig. 4. UV-vis DRS of prepared catalysts

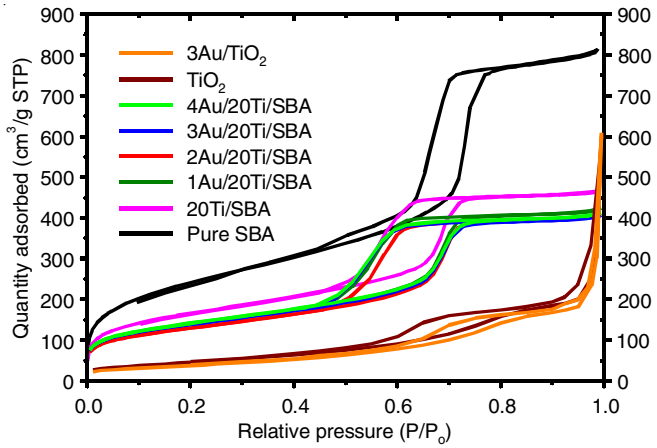

Fig. 5. Adsorption isotherms of prepared catalysts

area decreased from 872.9 m^2/g to 593.8 m^2/g for titania loaded sample. Pore volume also decreased correspondingly from 1.26 cm^3/g to 0.72 cm^3/g (Table-2). The pore diameter of titania modified and nanogold supported samples were comparable, which could be ascribed to the uniform dispersion of nanogold particles over TiO_2 nanoparticles. In case of TiO_2 and $3Au/TiO_2$ systems the surface area was found to be 160.3 and 139.6 m^2/g, respectively (Fig. 5).

XPS: The XPS core level spectra of nanogold incorporated titania modified SBA system for all the elements were calibrated for surface charging by referencing C 1s binding energy peak at 284.5 eV. The peaks nearly at 529.8 eV and 532.5 eV for O 1s represented the Ti-O-Ti and Si-O-Si bonds present in the system, respectively. The binding energy value of 103.4 eV for Si 2p was in agreement with earlier reports on SBA-15 (Fig. 6) [7]. The Au 4f core level spectra was deconvoluted into four peaks in which the peaks at binding energy values around 83.1 eV and 86.8 eV corresponded to $4f_{7/2}$ and $4f_{5/2}$ components of metallic gold and at 84.0 eV and 87.8 eV corresponded to that of gold in +1 oxidation state, respectively. The $4f_{7/2}$ and $4f_{5/2}$ doublets of the two spin orbit states of Au was separated by 3.7 eV. The relative percentage distribution of Au^0 (59.4%) was found to be higher than that of Au^{+1} (40.6%). The binding energy values of Ti at 458.7 eV and 464.4 eV represented the $2P_{3/2}$ and $2P_{1/2}$ components of octahedrally coordinated anatase TiO_2 (Fig. 6). The binding energy gap between the spin orbital multiplets of Ti 2p was found to be 5.7 eV which was in accordance with that of TiO_2 species reported in literature [19,20].

Catalytic activity studies: The catalytic performance of the nanogold supported systems was investigated in the liquid-phase reduction of 4-nitrophenol (4-NP) by $NaBH_4$ to 4-aminophenol (4-AP) as a model reaction. The catalytic activity for all the nanogold supported systems was tested for the reduction of 4-NP. The successive UV-vis absorption spectra for the catalytic reduction of 4-NP using all the nanogold supported systems are shown in Fig. 7.

The reaction kinetics was studied by plotting 2.303 log (a/a-x) against time of the reaction where 'a' is the initial absorbance and (a-x) is the absorbance in each time interval of the *p*-nitrophenolate ion. The reaction was found to be diffusion limited for the first few minutes. The plot gave a straight line by excluding the diffusion limits which indicated that the reaction followed pseudo first order kinetics (Fig. 8). From the plot, the rate constants were found to be $1.2 \times 10^{-3}\ s^{-1}$, $3.0 \times 10^{-3}\ s^{-1}$, $4.7 \times 10^{-3}\ s^{-1}$, $3.2 \times 10^{-3}\ s^{-1}$ for the catalysts 1Au/20Ti/SBA,

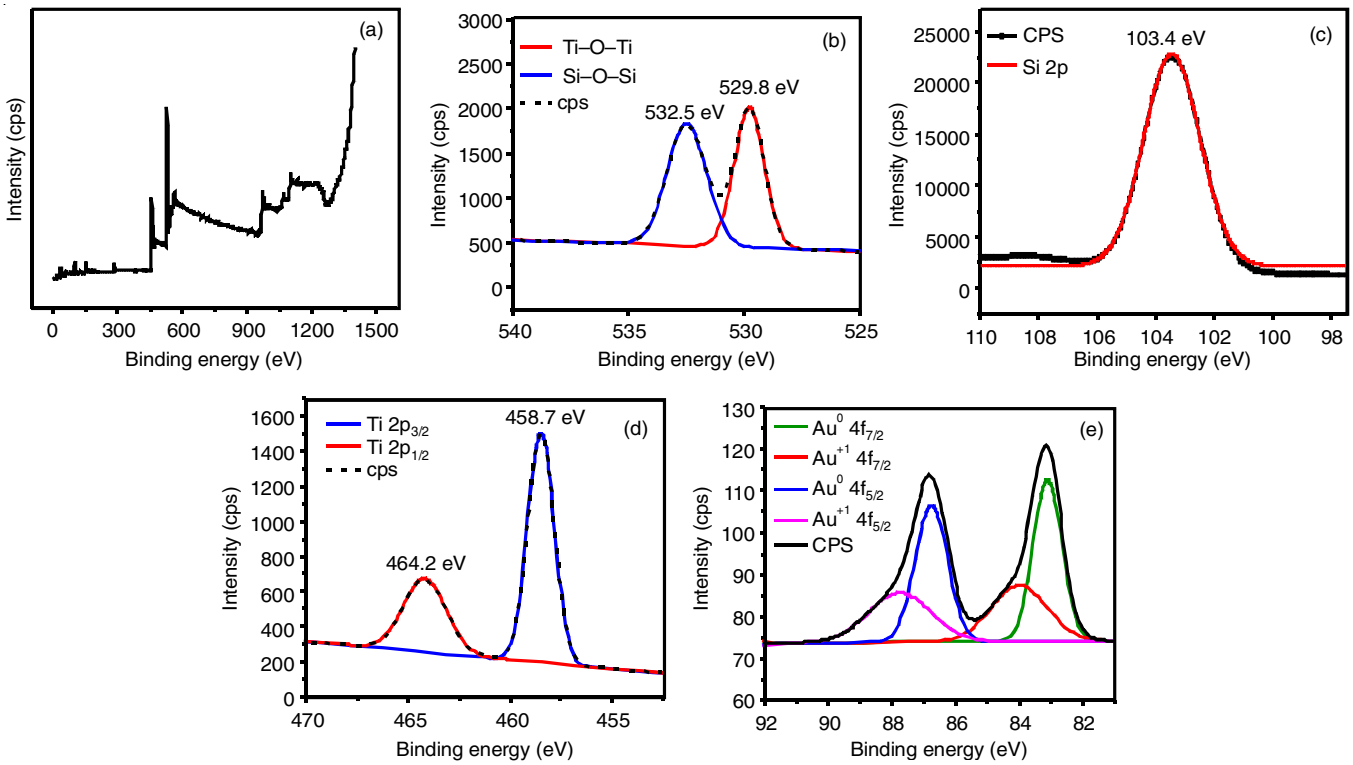

Fig. 6. Survey scan and core level spectra of nanogold dispersed titania loaded SBA system

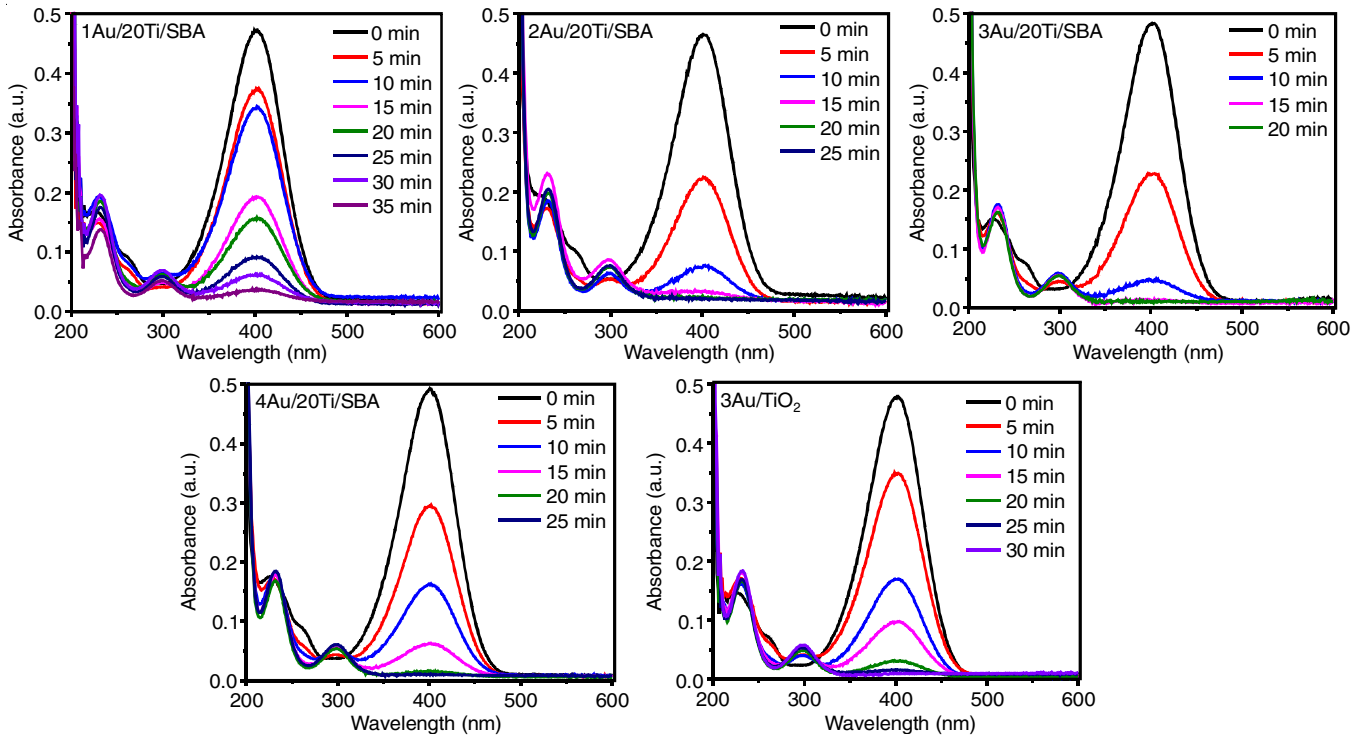

Fig. 7. Successive UV-vis absorption spectra of the reduction of 4-NP by $NaBH_4$ in the presence of nanogold supported catalysts (reaction conditions: 0.002 g XAu/20Ti/SBA, 3.3 mL of 0.32 M $NaBH_4$, 20 mL of 1 mmol 4-NP, 304 K, 300 rpm)

2Au/20Ti/SBA, 3Au/20Ti/SBA and 4Au/20Ti/SBA, respectively. The catalytic activity of $3Au/TiO_2$ system was also noted which showed a rate constant of $2.7 \times 10^{-3}\ s^{-1}$. The increased activity of 3Au/20Ti/SBA system over $3Au/TiO_2$ system could be attributed to the small particle size and efficient dispersion of nanogold over the high surface area Ti loaded silica support. The reaction was also conducted using hydrazine hydrate as the reducing agent in presence of 3Au/20Ti/SBA. The fact that the reaction did not occur in presence of hydrazine hydrate implied that the presence of a strong reducing agent is inevitable for the progress of the present catalytic reaction.

The effects of various parameters such as 4-NP concentration and agitation speed on reaction rate were investigated using 3Au/20Ti/SBA catalyst. The reaction rate decreased with increase in agitation speed (Table-3). This might be due to the decrease in effective concentration of the substrate in the solid/liquid interface.

The reaction rate decreased with increase in 4-NP concentration (Fig. 9). As the concentration of 4-NP increases, the catalyst surface will be mainly occupied by 4-NP molecules and thus the active sites become less accessible for borohydride molecules to get adsorbed. This would cause a reduction in

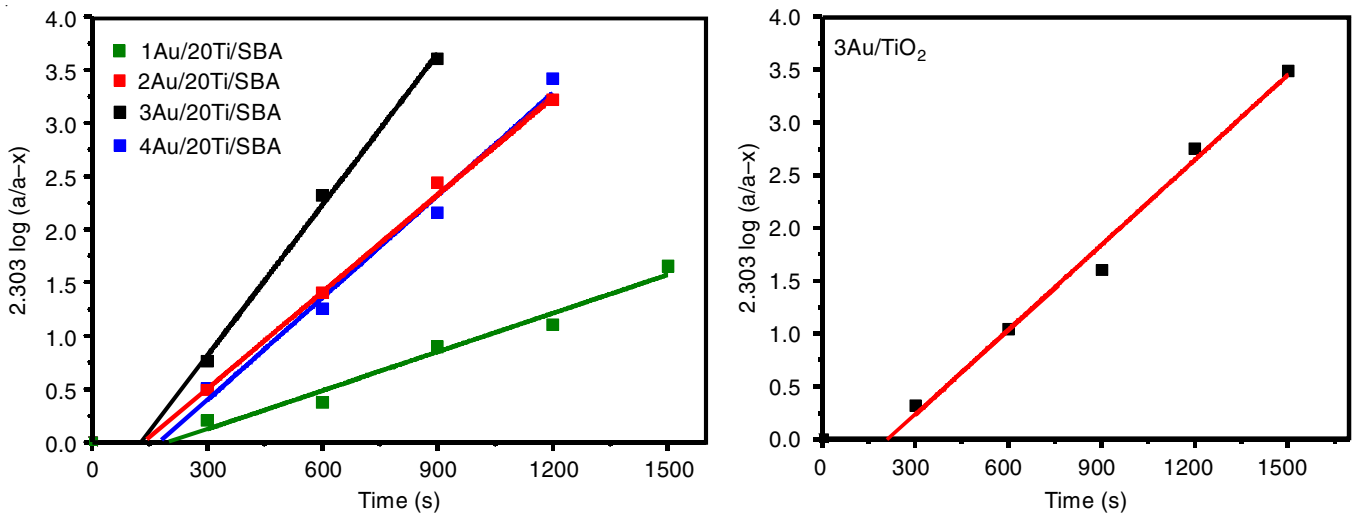

Fig. 8. Plots of 2.303 log (a/a-x) *versus* time for XAu/20Ti/SBA and $3Au/TiO_2$ (reaction conditions: 0.002 g catalyst, 3.3 mL of 0.32 M $NaBH_4$, 20 mL of 1 mmol 4-NP, 300 rpm, 304 K)

TABLE-3
EFFECT OF AGITATION SPEED ON THE RATE CONSTANT OF 4-NP REDUCTION REACTION

Agitation speed (rpm)	Rate constant ($\times 10^{-3}$ s^{-1})
300	4.7
600	4.3
900	2.7
1500	2.1

Reaction conditions: 0.002 g 3Au/20Ti/SBA, 3.3 mL of 0.32 M $NaBH_4$, 20 mL of 1 mmol 4-NP, 304 K

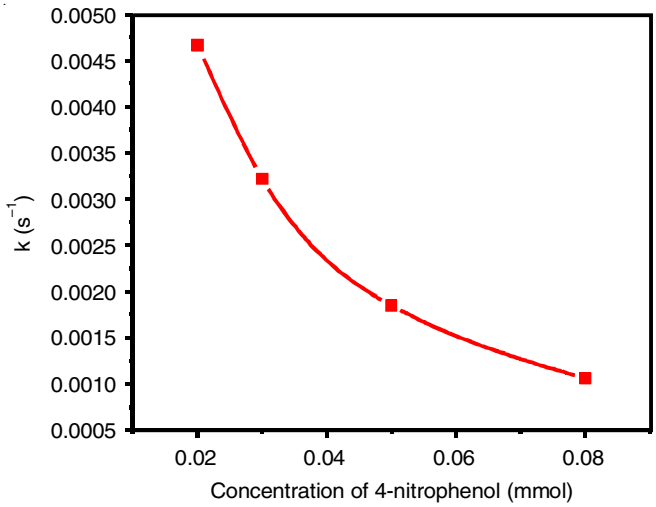

Fig. 9. Rate constants as a function of 4-NP concentration (reaction conditions: 0.002 g 3Au/20Ti/SBA, 3.3 mL of 0.32 M $NaBH_4$, 304 K, 300 rpm)

the reaction rate [1,21]. The reaction was monitored at different temperatures to find the activation energy (39.3 kJ/mol) (Fig. 10) which was found to be comparable with that of literature reports [22,23].

Table-4 shows the comparison of the results with literature reports. It is clearly evident that Au/4-NP ratio of 1/66 was lower than all the other reported systems. The ratio of Au/4-NP/$NaBH_4$ was 1/66/3470. The high activity of the present system compared to most of the reported system could be attributed to the combined effect of high surface area of the support SBA-15, catalytically active anatase phase of titania, small particle size of nanogold (average particle size < 5 nm) and its effective dispersion.

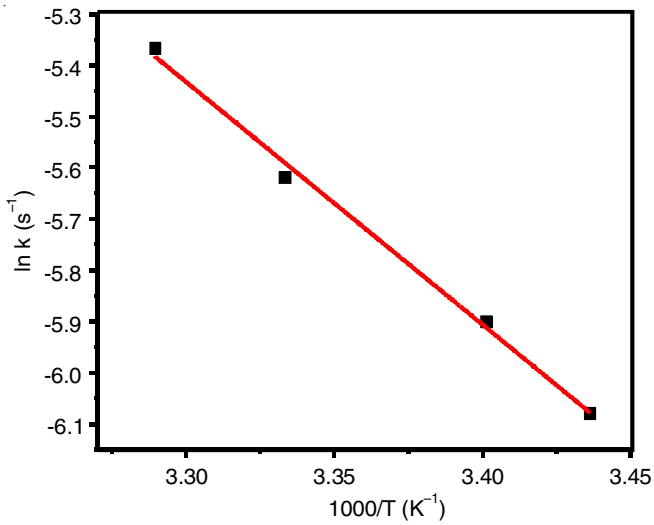

Fig. 10. Arrhenius plot of ln k *versus* 1/T for the reduction of 4-NP (reaction conditions: 0.002 g 3Au/20Ti/SBA, 3.3 mL of 0.32 M $NaBH_4$, 20 mL of 1 mmol 4-NP, 300 rpm)

Conclusion

Various weight percentages of nanogold dispersed TiO_2 loaded SBA-15 was prepared and characterized. From the TEM images, the particle size of gold in XAu/20Ti/SBA catalysts was found to be less than 5 nm. The weak diffraction lines in wide angle XRD indicated small particle size and efficient dispersion of gold nanoparticles on the support material. Surface plasmon resonance was evident from the diffuse reflectance UV-vis spectra of gold incorporated 20Ti/SBA catalyst which was characteristics of gold in the nano regime. The gold loaded titania modified SBA systems were tested for *p*-nitrophenol reduction using sodium borohydride. The increased activity of the nanogold supported Ti loaded silica systems over nanogold supported titania could be attributed to the efficient disper-

TABLE-4
COMPARISON OF THE CATALYTIC ACTIVITY IN THE REDUCTION OF 4-NITROPHENOL BETWEEN 3Au/20Ti/SBA AND VARIOUS SILICA SUPPORTED CATALYSTS REPORTED IN THE LITERATURE

Entry	Catalyst	σ (nm)	Au/4-NP/$NaBH_4$ approximate ratio	4-NP/$NaBH_4$ ratio	k ($s^{?1}$) $\times 10^{-3}$	Ref.
1	Au-SiO_2	12	1/25/9850	1/400	0.66	[24]
	Au-mSiO_2	12	1/25/9850	1/400	1.33	
2	Ni@Au NPs	8-18	1/2/1820	1/833	6.4	[25]
	Ni@Au/KCC-1	–	1/2/1820	1/833	8.3	
3	KCC-1–IL/Au	3.9	1/0.09/115	1/1337	12	[26]
4	Au@meso-SiO_2	20-80	–	1/400	1.3	[27]
5	1 CMC ND42-Au10.2 CMC	1-5	1/0.8/80	1/100	35	[28]
	ND42-Au1		1/0.8/80	1/100	25	
6	Au/m-SiO_2/Fe_3O_4	3.3	1/53/106200	1/2000	13	[29]
7	Au-20Co/SBA	–	1/1/3250	1/3300	---	[30]
8	AuNPs/SNTs	3-5	1/4/150	1/42	10.6	[31]
9	Au/γ-Fe_2O_3@SiO_2@KCC-1	5	1/6.4/530	1/83.5	14.5	[32]
10	Au_γ-CD NP	10.1	1/5/780	1/156	6.7	[33]
11	Au-CeO_2 catalyst	6.3	1/1/200	1/200	2.5	[34]
12	3Au/20Ti/SBA	< 5	1/66/3470	1/53	4.7	Present work

sion and small particle size of nanogold over the high surface area support.

ACKNOWLEDGEMENTS

The authors acknowledge their sincere gratitude to UGC, Government of India for the award of Junior Research Fellowship and Teacher fellowship under FDP scheme. Prof. B. Viswanathan, IIT Chennai and Dr. N. N. Binitha, University of Calicut are greatly acknowledged for their help and valuable suggestions. The authors also acknowledge SAIF CUSAT, India, St. Thomas College, Pala, CSMCRI, Bhavnagar, and Amrita Institute of Nano Sciences, Kochi, India for various analyses.

CONFLICT OF INTEREST

The authors declare that there is no conflict of interests regarding the publication of this article.

REFERENCES

1. Y.C. Chang and D.H. Chen, *J. Hazard. Mater.*, **165**, 664 (2009); https://doi.org/10.1016/j.jhazmat.2008.10.034
2. A.A. Ismail, A. Hakki and D.W. Bahnemann, *J. Mol. Catal. Chem.*, **358**, 145 (2012); https://doi.org/10.1016/j.molcata.2012.03.009
3. A.S. Hashimi, M.A.N.M. Nohan, S.X. Chin, S. Zakaria and C.H. Chia, *Nanomaterials*, **9**, 936 (2019); https://doi.org/10.3390/nano9070936
4. C. Kästner and A.F. Thünemann, *Langmuir*, **32**, 7383 (2016); https://doi.org/10.1021/acs.langmuir.6b01477
5. A.I. Ayad, D. Luart, A.O. Dris and E. Guénin, *Nanomaterials*, **10**, 1169 (2020); https://doi.org/10.3390/nano10061169
6. S. Varshney, D. Meyerstein, R. Bar-Ziv and T. Zidki, *Molecules*, **28**, 6530 (2023); https://doi.org/10.3390/molecules28186530
7. F. Rizzi, R. Castaldo, T. Latronico, P. Lasala, G. Gentile, M. Lavorgna, M. Striccoli, A. Agostiano, R. Comparelli, N. Depalo, M.L. Curri and E. Fanizza, *Molecules*, **26**, 4247 (2021); https://doi.org/10.3390/molecules26144247
8. S. Singh, A. Kumar, L. Nebhani and C.K. Hazra, *JACS Au*, **3**, 3400 (2023); https://doi.org/10.1021/jacsau.3c00563
9. H. Zhu, B. Lee, S. Dai and S.H. Overbury, *Langmuir*, **19**, 3974 (2003); https://doi.org/10.1021/la027029w
10. R. Zanella, A. Sandoval, P. Santiago, V.A. Basiuk and J.M. Saniger, *J. Phys. Chem. B*, **110**, 8559 (2006); https://doi.org/10.1021/jp060601y
11. A. Ghosh, C. Ranjan Patra, P. Mukherjee, M. Sastry and R. Kumar, *Micropor. Mesopor. Mater.*, **58**, 201 (2003); https://doi.org/10.1016/S1387-1811(02)00626-1
12. N. Petkov, N. Stock and T. Bein, *J. Phys. Chem. B*, **109**, 10737 (2005); https://doi.org/10.1021/jp050429i
13. L.-F. Gutierrez, S. Hamoudi and K. Belkacemi, *Appl. Catal. A Gen.*, **425–426**, 213 (2012); https://doi.org/10.1016/j.apcata.2012.03.025
14. S. Parambadath and A.P. Singh, *Catal. Today*, **141**, 161 (2009); https://doi.org/10.1016/j.cattod.2008.04.003
15. Z. Wang, Y. Xie and C.J. Liu, *J. Phys. Chem. C*, **112**, 19818 (2008); https://doi.org/10.1021/jp805538j
16. D. Zhao, J. Feng, Q. Huo, N. Melosh, G.H. Fredrickson, B.F. Chmelka and G.D. Stucky, *Science*, **279**, 548 (1998); https://doi.org/10.1126/science.279.5350.548
17. S. Mondal, M.E. De Anda Reyes and U. Pal, *RSC Adv.*, **7**, 8633 (2017); https://doi.org/10.1039/C6RA28640B
18. X. Li, S. Huang, Q. Xu and Y. Yang, *Transition Met. Chem.*, **34**, 943 (2009); https://doi.org/10.1007/s11243-009-9285-x
19. P. Babelon, A.S. Dequiedt, H. Mostefa-Sba, S. Bourgeois, P. Sibillot and M. Sacilotti, *Thin Solid Films*, **322**, 63 (1998); https://doi.org/10.1016/S0040-6090(97)00958-9
20. S. Bourgeois, P. le Seigneur and M. Perdereau, *Surf. Sci.*, **328**, 105 (1995); https://doi.org/10.1016/0039-6028(95)00022-4
21. B.M. Mogudi, P. Ncube, N. Bingwa, N. Mawila, S. Mathebula and R. Meijboom, *Appl. Catal. B*, **218**, 240 (2017); https://doi.org/10.1016/j.apcatb.2017.06.045
22. K. Kuroda, T. Ishida and M. Haruta, *J. Mol. Catal. Chem.*, **298**, 7 (2009); https://doi.org/10.1016/j.molcata.2008.09.009
23. Y. Khalavka, J. Becker and C. Sonnichsen, *J. Am. Chem. Soc.*, **131**, 1871 (2009); https://doi.org/10.1021/ja806766w
24. Y. Peng, W. Leng, B. Dong, R. Ge, H. Duan and Y. Gao, *Chin. J. Catal.*, **36**, 1117 (2015); https://doi.org/10.1016/S1872-2067(14)60310-7
25. X. Le, Z. Dong, W. Zhang, X. Li and J. Ma, *J. Mol. Catal. Chem.*, **395**, 58 (2014); https://doi.org/10.1016/j.molcata.2014.08.002
26. H. Yang, S. Li, X. Zhang, X. Wang and J. Ma, *J. Mater. Chem. A Mater. Energy Sustain.*, **2**, 12060 (2014); https://doi.org/10.1039/C4TA01513D
27. J. Chen, Z. Xue, S. Feng, B. Tu and D. Zhao, *J. Colloid Interface Sci.*, **429**, 62 (2014); https://doi.org/10.1016/j.jcis.2014.05.005
28. W. Wang, Z. Meng, Q. Zhang, X. Jia and K. Xi, *J. Colloid Interface Sci.*, **418**, 1 (2014); https://doi.org/10.1016/j.jcis.2013.11.043
29. H. Liu, C. Lin, Z. Ma, H. Yu and S. Zhou, *Molecules*, **18**, 14258 (2013); https://doi.org/10.3390/molecules181114258
30. S.P. Viswanathan, B.N. Narayanan, Z. Yaakob, S. Padikkaparambil and M. Mohammad, *React. Kinet. Mech. Catal.*, **111**, 335 (2014); https://doi.org/10.1007/s11144-013-0645-3
31. Z. Zhang, C. Shao, P. Zou, P. Zhang, M. Zhang, J. Mu, Z. Guo, X. Li, C. Wang and Y. Liu, *Chem. Commun.*, **47**, 3906 (2011); https://doi.org/10.1039/c0cc05693f
32. Z. Dong, G. Yu and X. Le, *New J. Chem.*, **39**, 8623 (2013); https://doi.org/10.1039/C5NJ00713E
33. S. Noel, H. Bricout, A. Addad, C. Sonnendecker, W. Zimmermann, E. Monflier and B. Leger, *New J. Chem.*, **44**, 21007 (2020); https://doi.org/10.1039/D0NJ03687K
34. T. Gia-Thien Ho, B.L. Do, B.V. Pham, T.T.V. Nguyen, H.P. Phan, H.B. Nguyen, P.P.T. Vo and N. Tri, *RSC Adv.*, **12**, 25753 (2022); https://doi.org/10.1039/D2RA04557E